

EPR study of Fe^{3+} in α -quartz: A reexamination of the lithium-compensated center

L. E. Halliburton and M. R. Hantehzadeh

Department of Physics, Oklahoma State University, Stillwater, Oklahoma 74078

J. Minge*

Department of Chemistry, University of Saskatchewan, Saskatoon, Saskatchewan, Canada S7N 0W0

M. J. Mombourquette

Department of Physics, Oklahoma State University, Stillwater, Oklahoma 74078
and *Department of Chemistry, University of Saskatchewan, Saskatoon, Saskatchewan, Canada S7N 0W0*

J. A. Weil

Department of Chemistry, University of Saskatchewan, Saskatoon, Saskatchewan, Canada S7N 0W0

(Received 31 January 1989)

X-band electron paramagnetic resonance (at ca. 20 K) and lithium-7 electron-nuclear double resonance (at ca. 4 K) studies of a lithium-compensated Fe^{3+} ($S = \frac{5}{2}$) center in synthetic iron-doped α -quartz have been carried out. The spin-Hamiltonian parameters were determined, allowing anisotropy of the g factor, as well as $[g, D, A(^7\text{Li}), P(^7\text{Li})]$ -matrix noncoaxiality, and including high-spin terms of the form S^4 . The data analysis confirms the model of the center (called S_1 by some workers) in which the Fe^{3+} ion occurs substitutionally at a Si^{4+} site, with charge compensation provided by an interstitial lithium +1 ion lying nearby on the same crystal twofold axis. The designation $[\text{FeO}_4/\text{Li}]^0$ is proposed for the center.

I. INTRODUCTION

We have recently undertaken a series of detailed electron paramagnetic resonance (EPR) and electron-nuclear double resonance (ENDOR) studies of several Fe^{3+} paramagnetic centers in crystalline α -quartz (SiO_2).^{1,2} Although in the past some of these Fe^{3+} centers were investigated and described, we believe that our recent theoretical and computational achievements not only result in a considerably more quantitative description of the spectra, but also allow elucidation of certain peculiarities of their structure.

In this paper we report the results of experiments on the lithium-compensated Fe^{3+} center $[\text{FeO}_4/\text{Li}]^0$ in synthetic iron-doped crystals. (See note added in proof.) This defect also occurs frequently in natural amethyst and citrine quartz crystals. The approximate spin Hamiltonian for this center [sometimes called S_1 (Refs. 1–6)] has been previously described by Hutton⁷ and Barry *et al.*⁸ by means of fine-structure parameters D , E , and F and assuming an isotropic g value. A barely resolvable four-line hyperfine structure was reported.⁸ However, no detailed experimental data on the compensating ion have yet been published. Our data, presented here, confirm a model of this center in which an Fe^{3+} ion substitutes for a Si^{4+} ion in quartz (C_2 local symmetry) with the charge-compensating Li^+ ion lying nearby (ca. 2.7 Å) on the same twofold axis (at least on the EPR time scale).

II. EXPERIMENTAL

The yellow-brown iron-doped (ca. 50 ppm Fe/Si) crystalline cultured quartz used in this investigation was grown by Sawyer Research Products (Lakeland, Ohio). Using the crystal morphology, the plate (ca. $10 \times 2 \times 3$ mm³) used was cut out of the original crystal such that the edges correspond to orthogonal axes $\hat{X} \parallel \hat{a}_1$ (a twofold axis), \hat{Y} , and $\hat{Z} \parallel \hat{c}$ (a threefold screw axis). To describe a general orientation of the external magnetic field vector \hat{B} relative to the \hat{X} , \hat{Y} , and \hat{Z} axes, polar angle θ and azimuthal angle φ are used, where $\theta = \angle(\hat{Z}, \hat{B})$ and $\varphi = \angle(\hat{X}, \text{projection of } \hat{B} \text{ onto the plane } XY)$. The sample was mounted in the EPR cavity such that \hat{a}_1 was perpendicular to $\mathbf{B} = B\hat{B}$.

The EPR lines from the symmetry-related sites⁹ were used to orient the plate accurately ($\pm 1'$). Here, symmetry-related sites 1, 2, and 3 correspond to $[\text{FeO}_4/\text{Li}]^0$ centers located on the three equivalent twofold axes \hat{a}_1 , \hat{a}_2 , and \hat{a}_3 , respectively. The sense of crystal rotation was checked by recording EPR lines of the previously described $[\text{FeO}_4/\text{H}]^0$ center,² which was also present in our sample, although at a much lower concentration. An EPR line-position data set was collected at 20 K using a low-temperature EPR cavity system¹⁰ and a Varian V4502 spectrometer operated at a fixed frequency of ca. 9.92 GHz. Rotation data were collected basically in 10° steps at angles measured with a precision of $\pm 1'$, over a 180° range in the plane $\hat{B} \perp \hat{a}_1$. All observable tran-

sitions (see Fig. 1) were explored, with special attention paid at the line-position turning points. Our frequency values and line-position field data had estimated uncertainties of 1×10^{-6} GHz and 1×10^{-3} mT, respectively. The magnetic field B was measured using a proton NMR gaussmeter. To take into account the difference in position between the NMR probe and the quartz sample, a small correction linear in B was applied. The correction coefficients were found through accurate measurements of several gas-phase dioxygen EPR lines, at known microwave frequency.¹¹

The EPR lines for the $[\text{FeO}_4/\text{Li}]^0$ center were clearly visible from 20 K to room temperature and showed no qualitative changes in that range. At the low temperatures, the EPR lines for this center tend to be easily power saturated, as was particularly observed on the so-called looping transitions (e.g., see Figs. 1 and 2).

At most orientations, the primary fine-structure EPR lines of $[\text{FeO}_4/\text{Li}]^0$ show poorly resolved hyperfine structure. These peaks originate from ^7Li nuclear-spin ($I = \frac{3}{2}$, 92.5% abundance) interaction with the unpaired electrons of the central Fe^{3+} ion.

Each fine-structure line is generally flanked by a pair of satellites showing splittings of ca. 1.1 mT. The intensity of these satellites relative to the main lines corresponds to the ratio of the abundance of the ^{57}Fe ($I = \frac{1}{2}$, 2.15% abundance) to the other (spinless) iron isotopes, so that the flanking lines may be considered to be a ^{57}Fe hyperfine doublet. A detailed study of the ^{57}Fe hyperfine

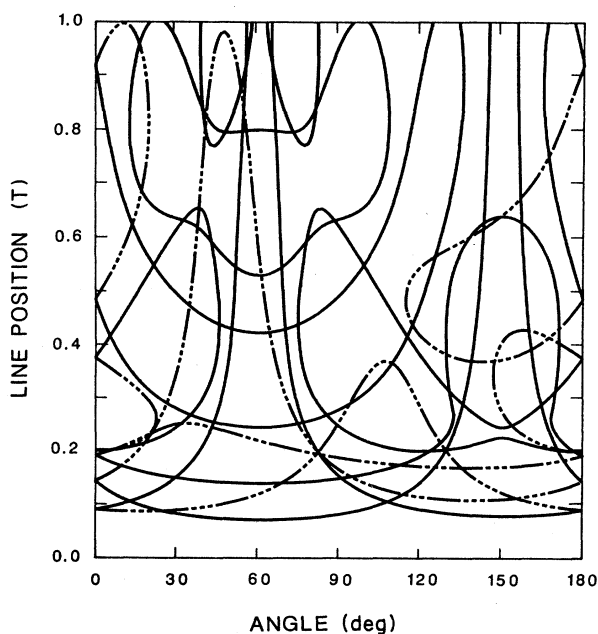


FIG. 1. EPR line positions at 9.915 GHz and $T=20$ K as a function of crystal rotation about twofold axis \hat{a}_1 . All symmetry-related sites are included; solid curves, site 1; dot-dash curves, sites 2 and 3. The ^7Li hyperfine structure is not discernible on the field scale used. Angle 0° is at $\hat{B} \parallel \hat{c}$, and 90° is at $\hat{B} \parallel \hat{Y}$ ($\hat{1}\hat{a}_1$ and \hat{c}).

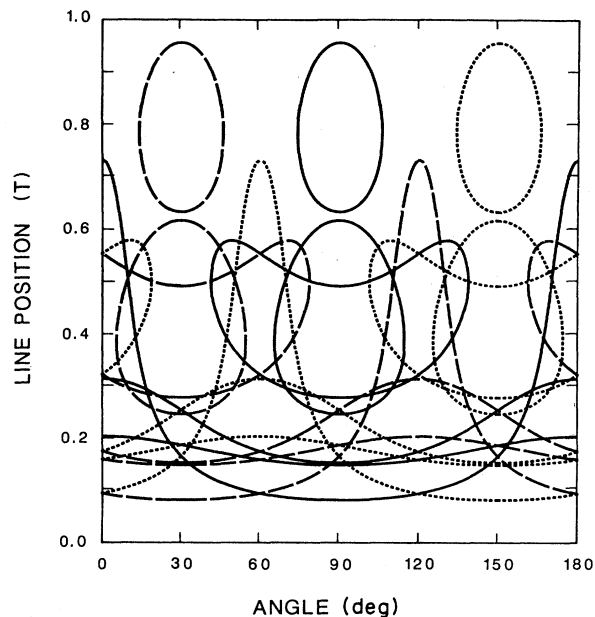


FIG. 2. EPR line positions at 9.915 GHz and $T=20$ K as a function of crystal rotation about threefold screw symmetry axis \hat{c} . All symmetry-related sites are included; solid curves, site 1; dashed curves, site 2; dotted curves, site 3. Angle 0° is at $\hat{B} \parallel \hat{a}_1$, and 90° is at $\hat{B} \parallel \hat{Y}$.

structure will be presented elsewhere.¹²

In addition, at some orientations, a second pair of weak satellites flanking the primary spectrum is observable. This doublet (with a splitting of ca. 0.22 mT) was shown to arise from ^{29}Si ($I = \frac{1}{2}$, 4.67% abundance), as discussed in the following.

Electron nuclear double resonance measurements were made using a Bruker ER200 EPR spectrometer with a model 250 ENDOR accessory. The data-acquisition system used is an Aspect 2000 computer interfaced with the spectrometer. The ENDOR cavity resonated in the TM_{011} mode. The radiofrequency magnetic field at the sample was created using a helix mounted on a quartz variable-temperature Dewar inserted into the microwave cavity, allowing for a wide range (0.5–100 MHz) of operating frequencies, with frequency-modulation depths up to 500 kHz. The ENDOR sample was cooled to ca. 4 K by an Oxford EPR-900 continuous-flow system. Because accurate alignment of the crystal could not be achieved in the ENDOR cavity, EPR spectra were taken at each orientation, along with the ENDOR spectra, and the previously determined spin-Hamiltonian parameters were utilized to calculate the actual crystal orientation.

The spin Hamiltonian used for $[\text{FeO}_4/\text{Li}]^0$ is similar to the one described by Mombourquette *et al.*¹ for $[\text{FeO}_4]^-$; in fact both centers have the same (C_2) symmetry. To describe the ^7Li effects, a hyperfine term of the forms $\mathbf{S} \cdot \mathbf{A} \cdot \mathbf{I}$, a nuclear quadrupole term $\mathbf{I} \cdot \mathbf{P} \cdot \mathbf{I}$, and an isotropic nuclear Zeeman term $-g_{\text{Li}} \beta_n \mathbf{I} \cdot \mathbf{B}$ were added. Appropriate symmetry constraints were used (to set certain of the

TABLE I. $[\text{FeO}_4/\text{Li}]^0$ principal values and directions of matrices $\mathbf{Y}=\mathbf{g}$ and \mathbf{D} in the crystal Cartesian coordinate system [Ref. 1, Table II: coordinate system (1); note that any principal direction defined by angles θ_k and φ_k equivalently can be described by angles $\theta'_k = 180^\circ - \theta_k$ and $\varphi'_k = 180^\circ + \varphi_k$] for site 1 at ca. 20 K, derived from the EPR data. The S^4 parameters B_4^m are included (Ref. 1). The estimated uncertainties are given in parentheses.

				Y	k	Y_k	θ_k	φ_k
\mathbf{g}								
	2.004 26(49)	0	0		1	2.004 26(49)	90	0
		2.003 70(21)	0.000 22(11)		2	2.004 18(17)	25.0(12.0)	90
			2.004 08(19)		3	2.003 60(19)	115.0(12.0)	90
\mathbf{D}/h (MHz)								
	-1399.79(51)	0	0		1	6348.35(68)	119.699(3)	270
		3575.44(75)	4861.72(54)		2	-1399.79(51)	90	0
			-2929.91(72)		3	-4948.56(68)	29.699(3)	270
B_4^m/h (MHz)								
	B_4^0/h	0.513(15)						
	B_4^1/h	0	B_4^2/h	-1.238(55)	B_4^3/h	0	B_4^4/h	3.812(85)
	B_4^{-1}/h	3.800(80)	B_4^{-2}/h	0	B_4^{-3}/h	0.400(24)	B_4^{-4}/h	0

matrix elements and B_4^m parameters to zero; see Tables I and II) while performing the least-squares fitting of the experimentally observed EPR and/or ENDOR transitions. A powerful, recently updated computer program¹ involving exact diagonalization of the whole spin-Hamiltonian matrix was used for this purpose.

III. RESULTS AND DISCUSSION

We have accurately determined the spin-Hamiltonian parameters including matrices \mathbf{g} , \mathbf{D} , $\mathbf{A}({}^7\text{Li})$, and $\mathbf{P}({}^7\text{Li})$ as well as the parameters for terms of type S^4 (Tables I and II). Fitting with higher-order Zeeman terms, of the BS^3 and BS^5 type,¹ did not result in better fits. The matrices \mathbf{g} , \mathbf{D} , and the S^4 parameters were obtained from averaged EPR line positions (each taken as the center of gravity of the lithium hyperfine pattern, if observed). The final rms deviation between the [111] observed and calculated EPR line positions was 0.13 mT. No attempts were made to derive the ${}^7\text{Li}$ hyperfine matrix from the generally poorly resolved lithium hyperfine structure observed in the EPR spectra. That information was obtained solely from ENDOR data.

Initially, in carrying out the least-squares-fitting procedure, the average positions of each of the observed ENDOR triplets (caused by lithium quadrupolar splittings)

were used, together with the calculated crystal orientations, to obtain the ${}^7\text{Li}$ hyperfine matrix. This matrix then served as a starting parameter set to fit each individual ENDOR transition, while allowing the matrix elements of both \mathbf{A} and \mathbf{P} to be varied during the least-squares-minimization procedure. The final rms deviation for the 153 ENDOR transitions was 0.007 MHz (0.0003 mT).

The signs of the S^2 (\mathbf{D} matrix) and S^4 parameters are linked to the signs of \mathbf{A} and \mathbf{P} : Equally good final fits (with the same rms deviations) were obtained for the two parameter sets taken with opposite relative signs. However, since the uniaxiality parameter

$$b = [A_1 - (A_2 + A_3)/2]/(3h)$$

of the dipolar part of the $\mathbf{A}({}^7\text{Li})$ matrix should be positive,¹³ the set of spin-Hamiltonian parameters yielding $b > 0$ was chosen (Table II). Here A_i ($i=1,2,3$) are the principal values of $\mathbf{A}({}^7\text{Li})$ arranged in the order of decreasing absolute values, and h is Planck's constant.

Figure 3 shows an energy-level diagram as a function of magnetic field B , for $\hat{\mathbf{B}}\|\hat{\mathbf{C}}$, with the observed EPR transitions indicated. A corresponding simulated c -axis spec-

TABLE II. $[\text{FeO}_4/\text{Li}]^0$ principal values and directions of matrices $\mathbf{Y}=\mathbf{A}({}^7\text{Li})$ and $\mathbf{P}({}^7\text{Li})$ in the crystal Cartesian coordinate system [Ref. 1, Table II: coordinate system (1)] for site 1 at ca. 4 K, derived from the ENDOR data. The estimated uncertainties are included, in parentheses.

				Y	k	Y_k	θ_k	φ_k
$\mathbf{A}({}^7\text{Li})/h$ (MHz)								
	3.6599(33)	0	0		1	3.6599(33)	90	0
		-0.8686(13)	-0.1500(15)		2	-0.6010(16)	29.3(2)	270
			-0.6852(19)		3	-0.9528(14)	119.3(2)	270
$\mathbf{P}({}^7\text{Li})/h$ (MHz)								
	-0.0090(4)	0	0		1	-0.0211(4)	109.6(6)	270
		0.0173(5)	0.0105(4)		2	-0.0090(4)	90	0
			-0.0084(4)		3	0.0121(4)	19.6(6)	270

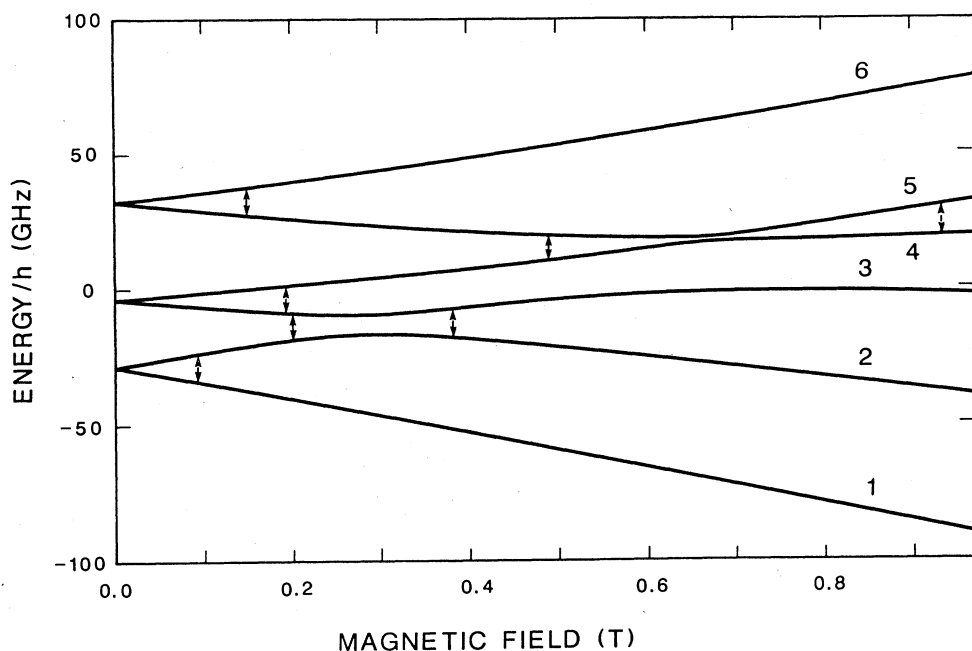


FIG. 3. The energy levels for $[\text{FeO}_4/\text{Li}]^0$ as a function of external magnetic field B ($\hat{\mathbf{B}}\|\hat{\mathbf{c}}$). No hyperfine splittings are included. Transitions at 9.915 GHz are indicated, and occur at (calculated) fields 90.34, 144.11, 192.12, 200.25, 375.31, 484.57, and 919.61 mT. The levels corresponding to the high-field m_s quantum numbers $-\frac{5}{2}$, $-\frac{3}{2}$, $-\frac{1}{2}$, $\frac{1}{2}$, $\frac{3}{2}$, and $\frac{5}{2}$ are numbered in order (increasing energy) from 1 to 6.

trum is presented in Fig. 4. The sets of all possible EPR line positions within the magnetic field range 0–1 T and for fixed microwave frequency 9.915 GHz are shown in Figs. 1 and 2 for rotation planes YZ and XY , respectively. The complexity of these “roadmaps” and especially the presence of looping transitions, as well as the energy-level

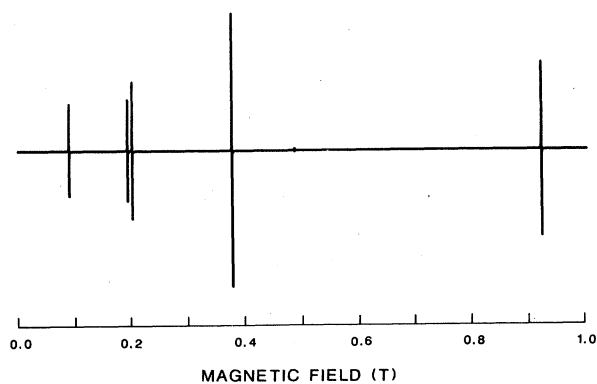


FIG. 4. EPR spectrum at 9.915 GHz simulated from the best-fit 20 K spin-Hamiltonian parameters in Table I, for $\hat{\mathbf{B}}\|\hat{\mathbf{c}}$ and excitation field $\hat{\mathbf{B}}_1\|\hat{\mathbf{a}}_1$. The transitions are also shown in Fig. 3. The ^7Li hyperfine splitting is not visible at the field scale used. The spectrum agrees well with the observed one; the line at 144.11 mT is not visible here due to its very small intensity.

diagram shown in Fig. 3, clearly indicate that the actual spin states cannot be considered, even in first approximation, to be pure eigenstates of the electron-spin-component operator \hat{S}_z (where $\hat{\mathbf{z}}\|\hat{\mathbf{B}}$). The contribution of the electronic quadrupole term $\mathbf{S}\cdot\mathbf{D}\cdot\mathbf{S}$ to the energy of each state is comparable to (and in fact even greater at some orientations than) that of the pure Zeeman term, in the magnetic-field region dealt with. Thus the usual perturbation approach (with the Zeeman spin Hamiltonian giving the unperturbed states) to calculate the state energies is quite inadequate in our case. Exact diagonalization is mandatory.

An observed and (exact) calculated EPR spectrum showing the best-resolved ^7Li hyperfine structure observable in the YZ plane is presented in Fig. 5. To simulate the outer “bumps” successfully, a pair of “clones” of the primary spectrum, less intense and separated by 0.22 mT, with intensity twice that corresponding to the natural abundance of ^{29}Si , were added to the primary spectrum. Thus, two symmetry-related nearby Si^{4+} ions giving rise to appreciable hyperfine splitting are seen to be present. An improved simulation of the central part of the spectrum was attained when the lines originating from the ^6Li isotope ($I=1$, 7.5% abundance) were also included. The line positions for the latter center were calculated using the same spin-Hamiltonian parameters as for the ^7Li case, except that the \mathbf{A} and \mathbf{P} matrix parameters were scaled, respectively, in accordance with the known $g(^6\text{Li})/g(^7\text{Li})$ and

$$\{Q(^6\text{Li})/[I(^6\text{Li})(2I(^6\text{Li})-1)]\} / \{Q(^7\text{Li})/[I(^7\text{Li})(2I(^7\text{Li})-1)]\}$$

ratios. The relative line intensities for the ^6Li and ^7Li spectra were derived from the ratio of their abundances. The simulation was done at experimental frequency 9.9147 GHz, assuming that all EPR lines have the same line width, $\Delta B_{p-p} = 0.030$ mT; the lineshapes used were for the Lorentzian first derivative. We note that the simulated spectrum is symmetrical, whereas the experimental one shows a slight asymmetry with respect to its center of gravity. This asymmetry can be simulated quite

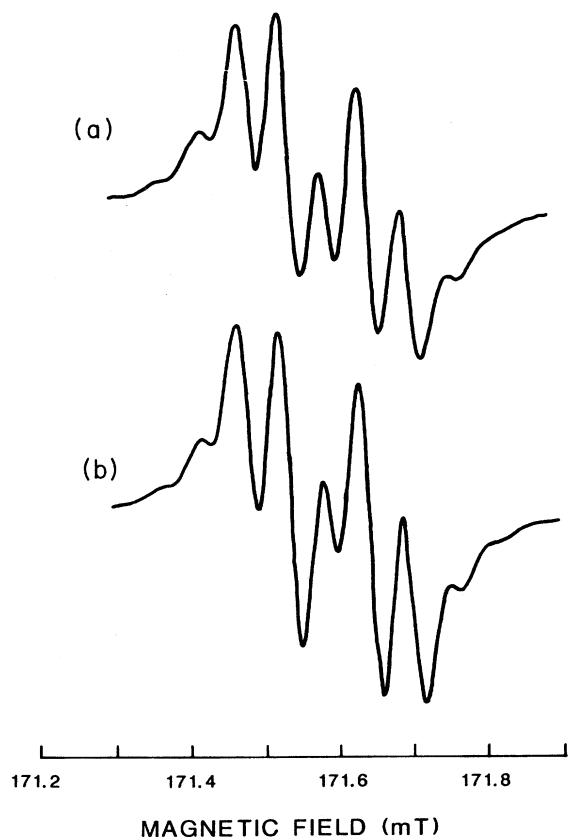


FIG. 5. First-derivative 20 K EPR spectrum (site 2) at 9.9147 GHz, showing the ^7Li hyperfine lines of the 3-4 ($m_s: -\frac{1}{2}-\frac{1}{2}$) transition at crystal orientation $\theta = 120^\circ$, $\varphi = 90^\circ$. (a) Experimental spectrum. (b) Spectrum simulated from the spin-Hamiltonian parameters of Tables I and II (see text). [The line positions for site 2 can be simulated using the matrices $\mathbf{Y}_{(1)}$ for site 1 (Tables I and II) transformed according to the formula $\mathbf{Y}_{(2)} = \mathbf{R}_{(2)} \cdot \mathbf{Y}_{(1)} \cdot \mathbf{R}_{(2)}^{-1}$, where

$$\mathbf{R}_{(2)} = \begin{bmatrix} -\frac{1}{2} & -3^{1/2}/2 & 0 \\ 3^{1/2}/2 & -\frac{1}{2} & 0 \\ 0 & 0 & 1 \end{bmatrix};$$

see Ref. 9.]

well if the ^6Li hyperfine spectrum is shifted towards lower magnetic field by ca. 0.01 mT as compared to the ^7Li one. Thus, it seems that the g , D , and S^4 parameters of the ^6Li -compensated Fe^{3+} center may differ slightly from those of the ^7Li species. On the other hand, the quality of the above-mentioned simulation implies that the spin-Hamiltonian parameters do not vary much within the temperature region 4–20 K; in fact, at ENDOR temperature (4 K), only three sites were observed at general orientation, indicating that the effective C_2 symmetry is preserved.

We note that all three principal g values are close to the free-electron value, and are very close to those of the $[\text{FeO}_4]^-$ center.¹ The g matrix is uniaxial (Table I), with the direction of its unique principal axis (corresponding to the smallest g value) not far from bisector \hat{w} ($\theta = 107.1^\circ$, $\varphi = 90.1^\circ$; see Table V of Ref. 1) of the $\text{Si}(0)-\text{O}_<(2)$ and $\text{Si}(0)-\text{O}_>(3)$ bonds. The second principal direction is close to bisector \hat{v}' ($\theta = 16.9^\circ$, $\varphi = 90.4^\circ$) and the third one is parallel to bisector \hat{u} (the twofold symmetry axis \hat{a}_1). The only major difference as compared to the $[\text{FeO}_4]^{-1}$ case is that the two principal directions perpendicular to the axis \hat{a}_1 correspond to interchanged g values.

The principal directions of matrix \mathbf{D} for $[\text{FeO}_4/\text{Li}]^0$ do not coincide with those of the g matrix, but seem to be related to them by a mirror reflection in the XZ plane. The two principal directions perpendicular to the \hat{a}_1 axis are very close to the planes (both sharing axis \hat{a}_1) containing the “short” bonds $\text{Si}-\text{O}_<$ and the “long” bonds $\text{Si}-\text{O}_>$, respectively (see Ref. 1). The direction corresponding to the largest D value makes an angle of 0.3° with the former plane; the direction for the smallest one is parallel to \hat{a}_1 .

The easiest to attain structural information about the $[\text{FeO}_4/\text{Li}]^0$ center is derivable from analysis of the dipolar part of $\mathbf{A}(^7\text{Li})$. This matrix has a relatively small isotropic part [$a_{\text{iso}} = \text{Tr } \mathbf{A} / (3h) = 0.7020(21)$ MHz] and is nearly uniaxial. The previously mentioned uniaxiality parameter b is 1.4789(16) MHz, whereas the asymmetry parameter $c = (A_2 - A_3) / (2h)$ is only 0.1759(15) MHz. The point-point dipolar model leads to a spin-spin distance of 2.75 Å. This is a reasonable value as compared to the calculated value for the Al—Li bond of 2.53 Å obtained by self-consistent-field-molecular-orbital (SCF-MO) calculation for the (diamagnetic) $[\text{AlO}_4/\text{Li}]^0$ center,¹⁴ or to the bond Si—Li of 2.65 Å obtained from similar calculations for the $[\text{SiO}_4/\text{Li}/\text{SiO}_4]^0$ center.¹⁵ This distance may also be compared directly with the pure α -quartz structural data, yielding 2.61 Å for the distance between atom $\text{Si}(0)$ and the nearby interstitial $a_>$ site.¹⁶ It is worth noting that the principal directions of matrix $\mathbf{A}(^7\text{Li})$ virtually coincide with the principal directions of \mathbf{D} , and are close also to those of matrix $\mathbf{P}(^7\text{Li})$.

Obviously, advanced quantum-mechanical cluster calculations for the $[\text{FeO}_4/\text{Li}]^0$ center will be required to fully interpret the present experimental results, but a tentative model for the center can be proposed. Judging

from the SCF-MO calculations for the $[\text{AlO}_4/\text{Li}]^0$ and $[\text{SiO}_4/\text{Li}/\text{SiO}_4]^0$ defects in α -quartz, it seems that the Li^+ ion is located close to the interstitial $a_{>}$ site (C_2 symmetry), where it coordinates "tetrahedrally" to the nearest four oxygen atoms, thus forming a $[\text{FeO}_4/\text{Li}/\text{SiO}_4]^0$ cluster. We note, however, that the average distance between the $a_{>}$ site and its neighboring oxygen atoms is ca. 2.01 Å, which is somewhat larger than the average Li—O bond length in other solids [compare, e.g., 1.92 Å in LiKSO_4 (Ref. 17) and 1.95 Å in $\text{Li}_2\text{SO}_4\cdot\text{H}_2\text{O}$ (Ref. 18)]. It seems then that the Li^+ ion exists in a relatively shallow potential minimum and jumps to the adjacent symmetry-related site frequently enough so that only its average position is observed on the EPR time scale (at least at ca. 4 K and above). Such a model explains why the $[\text{FeO}_4/\text{Li}]^0$ center shows C_2 symmetry down to ca. 4 K. By comparison, the 10 GHz EPR spectrum of the analogous sodium-compensated Fe^{3+} center, $[\text{FeO}_4/\text{Na}]^0$, shows a

crossover from the low-temperature C_1 symmetry to effective high-temperature C_2 symmetry at around 50 K. We expect to report a detailed study of that center soon.¹⁹

Note added in proof. With the discovery of a second type (denoted β) of center closely akin to the one discussed herein, we now call the center dealt with herein $[\text{FeO}_4/\text{Li}]^0_{\alpha}$.

ACKNOWLEDGMENTS

The authors wish to thank A. S. Nowick and J. J. Martin for making the samples available. This work was supported in part by the Natural Sciences and Engineering Research Council of Canada and by the U.S. Air Force under Contract No. FI9628-86-C-0138 with the Solid State Science Division, Rome Air Development Center, Hanscom Air Force Base.

*On leave from Institute of Molecular Physics, Polish Academy of Sciences, Poznań, Poland.

¹M. J. Mombourquette, W. C. Tennant, and J. A. Weil, *J. Chem. Phys.* **85**, 68 (1986).

²M. J. Mombourquette, J. Minge, M. R. Hantehzadeh, J. A. Weil, and L. E. Halliburton, *Phys. Rev. B* **39**, 4004 (1989).

³G. Lehmann and W. J. Moore, *J. Chem. Phys.* **44**, 1741 (1966).

⁴G. Lehmann, *Z. Naturforsch. A* **22**, 2080 (1967).

⁵W. Becker and G. Lehmann, *Solid State Commun.* **35**, 367 (1980).

⁶J. Seifarth, U. Bartuch, and W. Karthe, *Silikattechnik* **32**, 276 (1981).

⁷D. R. Hutton, *Phys. Lett.* **12**, 310 (1964).

⁸T. I. Barry, P. McNamara, and W. J. Moore, *J. Chem. Phys.* **42**, 2599 (1965).

⁹J. A. Weil, T. Buch, and J. E. Clapp, *Adv. Magn. Reson.* **6**, 183 (1973).

¹⁰B. D. Perlson and J. A. Weil, *Rev. Sci. Instrum.* **46**, 874

(1975).

¹¹M. Tinkham and M. W. P. Strandberg, *Phys. Rev.* **97**, 937 (1955); **97**, 951 (1955).

¹²J. Minge and J. A. Weil, *J. Phys. Chem. Solids* (to be published).

¹³M. J. Mombourquette and J. A. Weil, *J. Magn. Reson.* **66**, 105 (1986).

¹⁴M. J. Mombourquette and J. A. Weil, *Can. J. Phys.* **63**, 1282 (1985).

¹⁵T. M. Wilson, J. A. Weil, and P. S. Rao, *Phys. Rev. B* **34**, 6053 (1986).

¹⁶J. A. Weil, *Phys. Chem. Miner.* **10**, 149 (1984).

¹⁷S. Bhakay-Tamhane, A. Sequeira, and R. Chidambaram, *Acta Crystallogr.* **C40**, 1648 (1984).

¹⁸A. C. Larson, *Acta Crystallogr.* **18**, 717 (1965).

¹⁹L. E. Halliburton, M. R. Hantehzadeh, J. Minge, M. J. Mombourquette, and J. A. Weil (unpublished).